J|A|C|S ARTICLES

Published on Web 05/26/2010

# Molecular Mechanism of the Glycosylation Step Catalyzed by Golgi α-Mannosidase II: A QM/MM Metadynamics Investigation

Luis Petersen,[†] Albert Ardèvol,[‡,§] Carme Rovira,[‡,§,||] and Peter J. Reilly*[,†]

*Department of Chemical and Biological Engineering, Iowa State University, Ames, Iowa 50011, Computer Simulation and Modeling Laboratory (CoSMoLab), Parc Científic de Barcelona, 08028 Barcelona, Spain, Institut de Química Teòrica i Computacional (IQTCUB), Universitat de Barcelona, 08028 Barcelona, Spain, and Institució Catalana de Recerca i Estudis Avançats (ICREA), 08010 Barcelona, Spain*

Received November 9, 2009; E-mail: reilly@iastate.edu

***Abstract:*** Golgi α-mannosidase II (GMII), a member of glycoside hydrolase family 38, cleaves two mannosyl residues from $GlcNAcMan_5GlcNAc_2$ as part of the N-linked glycosylation pathway. To elucidate the molecular and electronic details of the reaction mechanism, in particular the conformation of the substrate at the transition state, we performed quantum mechanics/molecular mechanics metadynamics simulations of the glycosylation reaction catalyzed by GMII. The calculated free energy of activation for mannosyl glycosylation (23 kcal/mol) agrees very well with experiments, as does the conformation of the glycon mannosyl ring in the product of the glycosylation reaction (the covalent intermediate). In addition, we provide insight into the electronic aspects of the molecular mechanism that were not previously available. We show that the substrate adopts an $^{O}S_2/B_{2,5}$ conformation in the GMII Michaelis complex and that the nucleophilic attack occurs before complete departure of the leaving group, consistent with a $D_NA_N$ reaction mechanism. The transition state has a clear oxacarbenium ion (OCI) character, with the glycosylation reaction following an $^{O}S_2/B_{2,5} \rightarrow B_{2,5}$ [TS] $\rightarrow {}^{1}S_5$ itinerary, agreeing with an earlier proposal based on comparing α- and β-mannanases. The simulations also demonstrate that an active-site Zn ion helps to lengthen the $O2'-H_{O2'}$ bond when the substrate acquires OCI character, relieving the electron deficiency of the OCI-like species. Our results can be used to explain the potency of recently formulated GMII anticancer inhibitors, and they are potentially relevant in deriving new inhibitors.

## 1. Introduction

N-linked glycosylation is a post-translational process that attaches a carbohydrate to a nascent protein and further modifies it.[1] The process involves a series of well-defined carbohydrate trimming and addition steps performed by several glycoside hydrolases (GHs) and transferases, respectively, as described in the Supporting Information (SI) (Figure S1). The trimming steps start in the endoplasmic reticulum, followed by additional trimming and modification in the Golgi apparatus, where high-mannosyl oligosaccharides are converted to more complex ones.

Breast, colon, and skin cancer cells have an unusual distribution of cell-surface complex oligosaccharides, with increased GlcNAc branching on the trimannosyl core[2,3] correlated with disease progression.[4,5] Inhibition of Golgi α-mannosidase (GMII) with swainsonine blocks the abnormal formation of complex oligosaccharides, leading to reduced metastasis and tumor growth.[4,6] However, swainsonine also inhibits the closely related lysosomal α-mannosidase, limiting its clinical use.[4,7,8]

GMII cleaves α-1,3 and α-1,6 glycosidic bonds between mannopyranosyl residues in $GlcNAcMan_5GlcNAc_2$ (Figure 1).[9−11] Its amino acid sequence places it in GH family 38.[12,13] Several kinetic and crystallographic studies[11,14−20] have shown that the enzyme follows the general double-displacement mechanism of retaining GHs,[21] in which a covalent glycosyl-enzyme intermediate is formed. The mechanism consists of two steps. In the rate-limiting glycosylation step (Figure 2), a protonated carboxylate amino acid, Asp341 in *Drosphila melanogaster* GMII, transfers a proton to the oxygen atom of the scissile glycosidic bond. A second, negatively charged carboxylate amino acid, Asp204 in *Drosphila melanogaster* GMII, acts as the nucleophile, attacking the glycon C1′ atom to form a covalent intermediate with the protein. The type of coupling between the formation of the substrate-enzyme covalent

[†] Iowa State University.
[‡] Parc Científic de Barcelona.
[§] IQTCUB.
[||] ICREA.

(1) Roth, J. *Chem. Rev.* **2002**, *102*, 285–303.
(2) Yamashita, K.; Ohkura, T.; Tachibana, Y.; Takasaki, S.; Kobata, A. *J. Biol. Chem.* **1984**, *259*, 10834–10840.
(3) Pierce, M.; Arango, J. *J. Biol. Chem.* **1986**, *261*, 10772–10777.
(4) Goss, P. E.; Baker, M. A.; Carver, J. P.; Dennis, J. W. *Clin. Cancer Res.* **1995**, *1*, 935–944.
(5) Dennis, J. W.; Granovsky, M.; Warren, C. E. *Biochim. Biophys. Acta* **1999**, *1473*, 21–34.
(6) Goss, P. E.; Reid, C. L.; Bailey, D.; Dennis, J. W. *Clin. Cancer Res.* **1997**, *3*, 1077–1086.
(7) Elbein, A. D.; Solf, R.; Dorling, P. R.; Vosbeck, K. *Proc. Natl. Acad. Sci. U.S.A.* **1981**, *78*, 7393–7397.
(8) Bowen, D.; Adir, J.; White, S. L.; Bowen, C. D.; Matsumoto, K.; Olden, K. *Anticancer Res.* **1993**, *13*, 841–844.

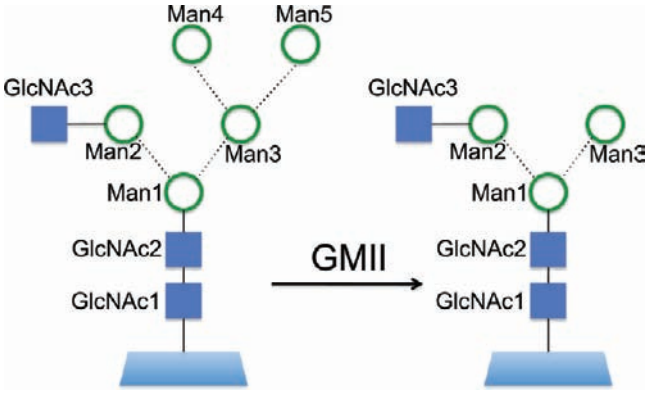


***Figure 1.*** Schematic of the GMII-catalyzed hydrolysis reaction. Bond configuration denoted by bond angle: 1,2: 90°; 1,3: 135°; 1,4: 180°; 1,6: 225°. Anomeric configuration: α, dashed lines; $\beta$, solid lines.[9]

bond and the scission of the substrate glycosidic bond determines whether the mechanism is $D_NA_N$, $A_ND_N$, $D_N{*}A_N$, or $D_N + A_N$ type.[22,23] This information has not been conclusively determined for GMII. The transition state (TS) of the reaction is oxacarbenium-ion like, but the conformation of the glycon sugar ring (mannose in GMII) varies among GHs.[24] In a second step (deglycosylation), a water molecule attacks the C1′ atom, breaking the covalent bond to finish the reaction and to regenerate the enzyme for the next catalytic round.

The available structural data on GMII is from *D. melanogaster*, which has kinetic and inhibition properties similar to those of mammalian GMII.[25] These two forms also have high sequence identity (41%),[15] their active-site amino acid residues being virtually identical. As observed in many other GHs,[24] it is expected that GMII binds the substrate in a distorted conformation. However, the precise conformation of the Man5 mannosyl residue in the GMII Michaelis complex is uncertain. Mutated GMII (D341N) forces a complexed mannose molecule into a near-$B_{2,5}$ conformation (PDB 3BUP) ($E_5/{}^{O}H_5$ from analysis of the puckering coordinates extracted from the crystal structure). Nevertheless, the authors warned that their assignment was not unambiguous and that other nearby puckering conformers, such as ${}^{O}S_2$ and ${}^{O}H_5$, could also be accommodated reasonably well.[19] A mannosyl residue in a branched substrate complexed with another mutated GMII structure (D204A) (PDB 3CZN) (Figure 3a) displays a regular ${}^4C_1$ conformation.[11] The conformation of the substrate in the product of the glycosylation reaction (the covalent intermediate in Figure 2) is more clear-cut, as crystal structures of wild-type GMII bound to fluorinated mannose analogs (PDB 1QX1, 1QWU, and 1QWN) consistently reveal distorted ${}^1S_5$ conformations.[16] By analogy with the conformational itinerary suggested for another mannose-cleaving enzyme (GH26 $\beta$-mannanase),[26] it has been proposed that the substrate mannosyl residue in GMII features a $B_{2,5}$-type of TS[16,19,24] and follows the ${}^{O}S_2 \rightarrow B_{2,5}$ [TS] $\rightarrow {}^1S_5$ itinerary for the glycosylation step. However, this proposal awaits further verification.

The active site of *D. melanogaster* GMII, complexed with its natural (branched) substrate (PDB 3CZN), is shown in Figure 3a. Asp341 is the catalytic acid/base residue (Figure 2), while Ala204 replaces the catalytic nucleophile (Asp204).[16,27] The active site also accommodates a catalytic zinc ion that coordinates two substrate glycon hydroxyl groups (C2′−OH and C3′−OH) and three residues (His90, Asp92, and His471). The presence of a catalytic zinc ion is unprecedented in GHs[28] and its precise role during catalysis is unclear. Several roles for the zinc ion have been proposed, including assisting in distorting the mannosyl (Man5) ring and in correctly orienting the nucleophile.[29]

Structural/electronic information for the glycosylation reaction TS, of interest in designing GMII inhibitors as anticancer agents, is very difficult to obtain experimentally. Computational approaches, in particular first-principles simulations, can be very useful to obtain this information, as exemplified by recent studies for other GH enzymes.[30−34] To the best of our knowledge, the catalytic mechanism of GMII has not yet been addressed by first-principles methods.

We report here a quantum mechanics/molecular mechanics (QM/MM) metadynamics simulation of the *D. melanogaster* GMII-catalyzed glycosylation reaction during α-1,6-mannosyl bond hydrolysis. Our study presents strong hypotheses regarding the molecular/electronic details of the mechanism, specifically the substrate conformation in the Michaelis complex, the conformational itinerary that the mannosyl ring substrate follows during catalysis, the type of mechanism, the role of the Zn ion during catalysis, and the structural/electronic properties of the TS.

(9) Tulsiani, D. R.; Hubbard, S. C.; Robbins, P. W.; Touster, O. *J. Biol. Chem.* **1982**, *257*, 3660–3668.
(10) Moremen, K. W.; Trimble, R. B.; Herscovics, A. *Glycobiology* **1994**, *4*, 113–125.
(11) Shah, N.; Kuntz, D. A.; Rose, D. R. *Proc. Natl. Acad. Sci. U.S.A.* **2008**, *105*, 9570–9575.
(12) Coutinho, P.; Henrissat, B. www.cazy.org, 1999.
(13) Cantarel, B. L.; Coutinho, P. M.; Rancurel, C.; Bernard, T.; Lombard, V.; Henrissat, B. *Nucleic Acids Res.* **2009**, *37*, 233–238.
(14) Numao, S.; He, S.; Evjen, G.; Howard, S.; Tollersrud, O. K.; Withers, S. G. *FEBS Lett.* **2000**, *484*, 175–178.
(15) van den Elsen, J. M.; Kuntz, D. A.; Rose, D. R. *EMBO J.* **2001**, *20*, 3008–3017.
(16) Numao, S.; Kuntz, D. A.; Withers, S. G.; Rose, D. R. *J. Biol. Chem.* **2003**, *278*, 48074–48083.
(17) Kuntz, D. A.; Ghavami, A.; Johnston, B. D.; Pinto, B. M. *Tetrahedron: Asymmetry* **2005**, *16*, 25–32.
(18) Kuntz, D. A.; Tarling, C. A.; Withers, S. G.; Rose, D. R. *Biochemistry* **2008**, *47*, 10058–10068.
(19) Zhong, W.; Kuntz, D. A.; Ember, B.; Singh, H.; Moremen, K. W.; Rose, D. R.; Boons, G. J. *J. Am. Chem. Soc.* **2008**, *130*, 8975–8983.
(20) Kuntz, D. A.; Zhong, W.; Guo, J.; Rose, D. R.; Boons, G. J. *Chembiochem* **2009**, *10*, 268–277.
(21) Koshland, D. E. *Biol. Rev. Camb. Phil. Soc.* **1953**, *28*, 416–436.
(22) Guthrie, R. D.; Jencks, W. P. *Acc. Chem. Res.* **1989**, *22*, 1161–1178.
(23) Schramm, V. L.; Shi, W. *Curr. Opin. Struct. Biol.* **2001**, *11*, 657–665.
(24) Vocadlo, D. J.; Davies, G. J. *Curr. Opin. Chem. Biol.* **2008**, *12*, 539–555.
(25) Rabouille, C.; Kuntz, D. A.; Lockyer, A.; Watson, R.; Signorelli, T.; Rose, D. R.; van den Heuvel, M.; Roberts, D. B. *J. Cell. Sci.* **1999**, *112*, 3319–3330.
(26) Ducros, V. M.; Zechel, D. L.; Murshudov, G. N.; Gilbert, H. J.; Szabo, L.; Stoll, D.; Withers, S. G.; Davies, G. J. *Angew. Chem., Int. Ed.* **2002**, *41*, 2824–2827.
(27) Howard, S.; He, S.; Withers, S. G. *J. Biol. Chem.* **1998**, *273*, 2067–2072.
(28) Vasella, A.; Davies, G. J.; Bohm, M. *Curr. Opin. Chem. Biol.* **2002**, *6*, 619–629.
(29) Kuntz, D. A.; Liu, H.; Bols, M.; Rose, D. R. *Biocatal. Biotransf.* **2006**, *24*, 55–61.
(30) Bottoni, A.; Miscione, G. P.; De Vivo, M. *Proteins* **2005**, *59*, 118–130.
(31) Bowman, A. L.; Grant, I. M.; Mulholland, A. J. *Chem. Commun. (Camb)* **2008**, 4425–4427.
(32) Petersen, L.; Ardevol, A.; Rovira, C.; Reilly, P. J. *J. Phys. Chem. B* **2009**, *113*, 7331–7339.
(33) Soliman, M. E.; Ruggiero, G. D.; Pernia, J. J.; Greig, I. R.; Williams, I. H. *Org. Biomol. Chem.* **2009**, *7*, 460–468.
(34) Soliman, M. E.; Pernia, J. J.; Greig, I. R.; Williams, I. H. *Org. Biomol. Chem.* **2009**, *7*, 5236–5244.

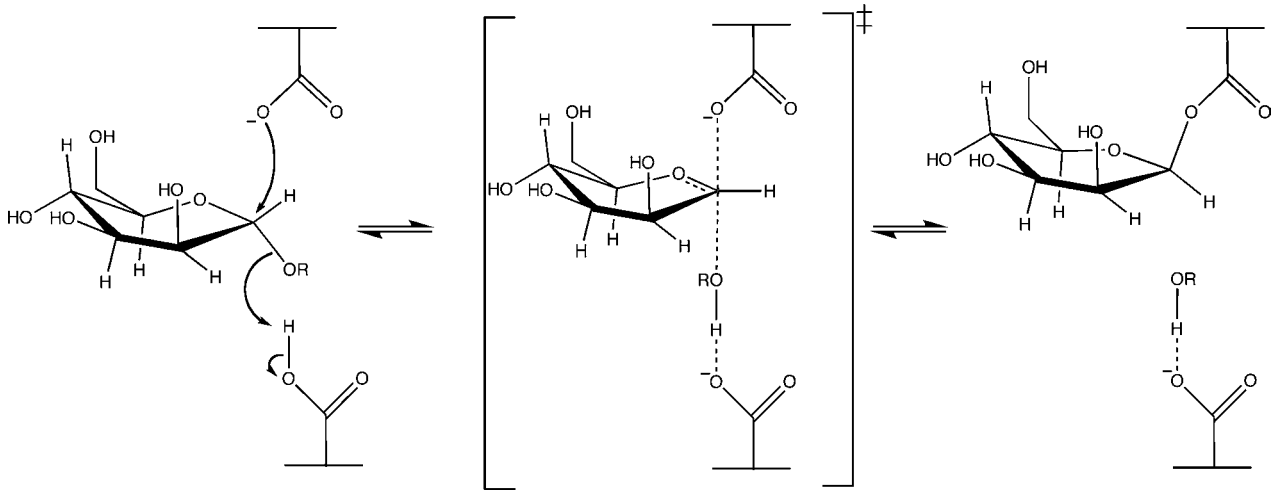

***Figure 2.*** Catalytic mechanism of the glycosylation step in retaining GHs. The nucleophile and acid/base residues of GMII are Asp204 and Asp341, respectively.

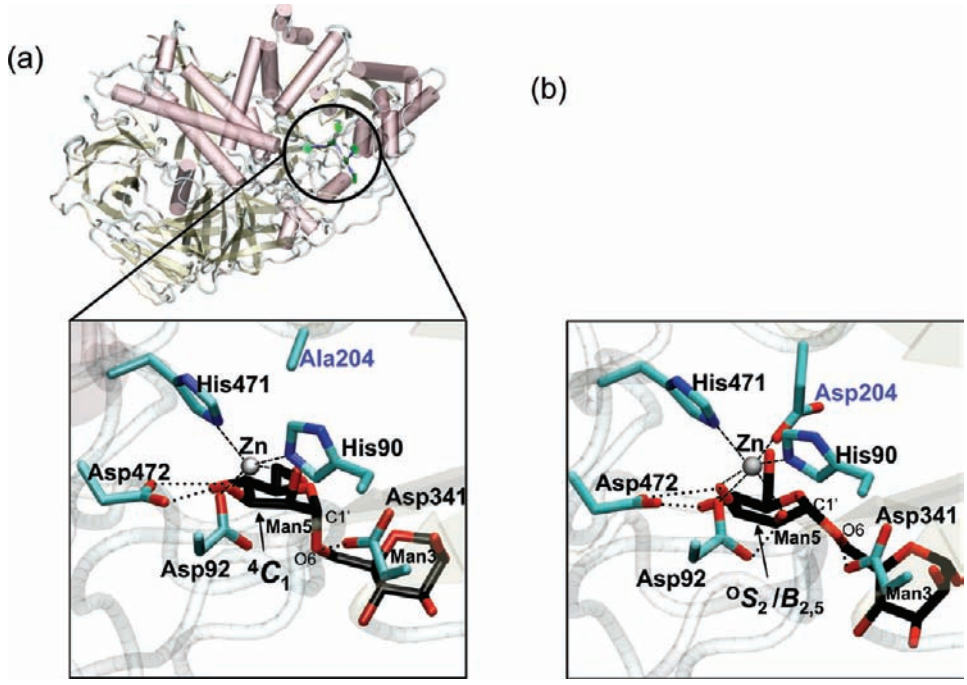


***Figure 3.*** Active site of GMII complexed with GlcNAcMan$_5$GlcNAc. (a) X-ray structure of the D204A mutant (PDB 3CZN), featuring a $^4C_1$ conformation of the Man5 substrate mannosyl ring. (b) Optimized structure of the native enzyme obtained from the QM/MM simulation after reverting the D204A mutation. The Man5 substrate mannosyl ring adopts a $^OS_2/B_{2,5}$ conformation.

## 2. Computational Methods

**2.1. Classical Molecular Dynamics Simulations.** The initial structure for the simulation was taken from a recently published crystallographic study of *D. melanogaster* GMII (PDB 3CZN, at 1.4 Å resolution) complexed with its natural substrate and with its catalytic nucleophile mutated (D204A).[11] The active site B-factors of this structure are presented in Table S1 (SI). The mutation was computationally reverted to Asp204, using other unmutated structures as a template, and hydrogen atoms were added using the AmberTools package.[35] The catalytic acid/base, Asp341, was modeled in its protonated state, while Asp204 was modeled in its deprotonated, charged state, consistent with the glycosylation step of the retaining mechanism. The protonation states and hydrogen atom positions of all other ionizable amino acid residues were selected based on their hydrogen bond network. Thirty-six histidine residues were modeled in their neutral states, while the rest were modeled in their charged states. All the crystallographic water molecules were retained and extra water molecules were added to form a 10-Å water box around the protein surface. Two chloride ions were also added to neutralize the enzyme charge.

The system was initially subjected to classical molecular dynamics (MD) using Amber9 software.[35] The protein and the Zn ion were modeled with the FF99SB force field,[36] (*i.e.*, the Zn ion interacts with its neighbors via electrostatic and van der Waals interactions). All carbohydrates, including the substrate and GlcNAc glycosylation site at Asn194, were modeled with the GLYCAM06

(35) Pearlman, D. A.; Case, D. A.; Caldwell, J.; Ross, W. S.; Cheatham, T. E.; DeBolt, S.; Ferguson, D.; Seibel, G.; Kollman, P. *Comput. Phys. Commun.* **1995**, *91*, 1–41.

(36) Hornak, V.; Simmerling, C. *Proteins* **2003**, *51*, 577–590.

force field.[37] Finally, all water molecules were described with the TIP3P force field.[38] The MD simulation was carried out in several steps. First the system was minimized, holding the protein and substrate fixed. Then the entire system was allowed to relax. To gradually reach the desired temperature of 300 K in the MD simulation, weak spatial constraints were initially added to the protein and substrate, while the water molecules and chloride ions were allowed to move freely. The constraints were then removed and the MD was extended to 1 ns when the system had reached equilibrium. Because the force field was unable to retain some important active-site hydrogen bonds, two distance constraints were used during the classical MD simulation, one between the proton of the catalytic acid/base and the glycosidic oxygen atom ($H_{Asp341}-O6$), which is important for the glycosylation reaction, and a second between Asp92 and the C2′−OH hydroxyl group ($H_{O2'}-O_{Asp92}$), a hydrogen bond experimentally observed in the structure of mutated GMII (D341N) complexed with mannose (PDB 3BUP).[19] The Zn ion maintained its 6-fold coordination during the classical simulation. A snapshot of the MD-equilibrated system was taken for the subsequent QM/MM and metadynamics simulations, which were performed without any constraint. A superposition between the equilibrated GMII structure (after QM/MM minimization) and the X-ray crystal structure is presented in Figure S2 (SI).

**2.2. QM/MM Metadynamics Simulations.** QM/MM calculations were performed using the method developed by Laio et al.,[39] which combines Car−Parrinello MD,[40] based on density functional theory (DFT), with force-field MD methodology. A detailed description of the QM/MM method can be found in the SI. Previous studies showed that this methodology provides an accurate description of energetic, dynamic, and structural features of biological systems, including GHs.[41,42]

The QM region chosen in this work included the side chains of His90, Asp92, Asp204, Asp341, and His471, capped at their Cα atoms with a link-atom pseudopotential, and two active-site mannosyl residues, Man3 and Man5 (Figure 3a), capped at the C1 atom of Man4 and the C6 atom of Man1, as well as the zinc ion. The QM region (92 atoms) was enclosed in an isolated 19.5 × 15.7 × 19.7 Å$^3$ supercell. Kohn−Sham orbitals were expanded in a plane-wave basis set with a kinetic energy cutoff of 80 Ry. Norm-conserving Troullier-Martins *ab initio* pseudopotentials[43] were used for all elements. For Zn, the d$^{10}$ semicore electrons were considered explicitly in the calculations. We used a pseudopotential with cutoff radii $r_s = 1.8$ au, $r_p = 2.0$ au, $r_d = 1.8$ au, which also incorporates scalar relativistic effects. The efficiency of the Zn pseudopotential has been previously tested against all-electron calculactions.[44]

The BLYP functional[45,46] in the generalized gradient-corrected approximation of DFT was selected in view of its good performance in previous works of Zn-containing enzymes such as alcohol dehydrogenase,[47] β-lactamase,[48] the zinc analogue of Synthetic Diiron Protein DF1,[49] endonuclease IV,[50] and thermolysin.[44] A recent study[51] on small Zn-containing compounds, however, concludes that other functionals (among them M05−2X,[52] B3LYP[53−55] and BP86[45,56]) perform better than BLYP. Additional calculations on a GMII model to test the dependence of our results on the functional employed (SI, pages S11−S15) show that relative energies, distances, and atomic charges are not significantly affected.

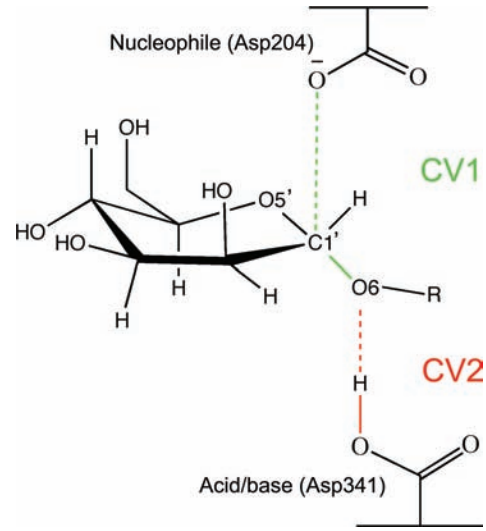


***Figure 4.*** Two collective variables of the system. CV1 models the $O_{Asp204}-C1'$ nucleophilic attack and the rupture of the C1′−O6 glycosidic bond. CV2 models the proton transfer between the acid/base amino acid residue (Asp341) and the glycosidic oxygen atom (O6).

A constant temperature of 300 K was reached by coupling the system to a Nosé-Hoover thermostat[57] at 3500 cm$^{-1}$. Structural optimizations were done by annealing ionic velocities until the maximal component of the nuclear gradient was $<10^{-4}$ au. A time step of 0.12 fs and a fictitious electron mass of 700 au were used in the Car−Parrinello simulations.

The metadynamics technique[58] was used to overcome energy barriers and to reconstruct the free energy landscape of the glycosylation reaction. The general details of this method are described in the SI. The collective variables (CVs) used in this work were taken as a combination of coordination indices of the covalent bonds being formed/broken (Figure 4). Each CV is the difference of coordination number (CN)[59] of two bonds (more generally defined in the SI) and is given by

$$\mathrm{CN}_{ij} = \frac{1 - (d_{ij}/d^0)^p}{1 - (d_{ij}/d^0)^{p+q}}$$

(37) Kirschner, K. N.; Yongye, A. B.; Tschampel, S. M.; Gonzalez-Outeirino, J.; Daniels, C. R.; Foley, B. L.; Woods, R. J. *J. Comput. Chem.* **2008**, *29*, 622–655.
(38) Jorgensen, W.; Chandrasekhar, J.; Madura, J.; Impey, R.; Klein, M. *J. Chem. Phys.* **1983**, *79*, 926–935.
(39) Laio, A.; VandeVondele, J.; Rothlisberger, U. *J. Chem. Phys.* **2002**, *116*, 6941–6947.
(40) Car, R.; Parrinello, M. *Phys. Rev. Lett.* **1985**, *55*, 2471–2474.
(41) Carloni, P.; Rothlisberger, U.; Parrinello, M. *Acc. Chem. Res.* **2002**, *35*, 455–464.
(42) Dal Peraro, M.; Ruggerone, P.; Raugei, S.; Gervasio, F. L.; Carloni, P. *Curr. Opin. Struct. Biol.* **2007**, *17*, 149–156.
(43) Troullier, N.; Martins, J. L. *Phys. Rev. B Condens. Matter* **1991**, *43*, 1993–2006.
(44) Blumberger, J.; Lamoureux, G.; Klein, M. L. *J. Chem. Theory Comput.* **2007**, *3*, 1837–1850.
(45) Becke, A. D. *Phys. Rev. A* **1988**, *38*, 3098–3100.
(46) Lee, C.; Yang, W.; Parr, R. G. *Phys. Rev. B: Condens. Matter Mater. Phys.* **1988**, *37*, 785–789.
(47) Gervasio, F. L.; Schettino, V.; Mangani, S.; Krack, M.; Carloni, P.; Parrinello, M. *J. Phys. Chem. B* **2003**, *107*, 6886–6892.
(48) Dal Peraro, M.; Llarrull, L. I.; Rothlisberger, U.; Vila, A. J.; Carloni, P. *J. Am. Chem. Soc.* **2004**, *126*, 12661–12668.
(49) Magistrato, A.; DeGrado, W. F.; Laio, A.; Rothlisberger, U.; Vande-Vondele, J.; Klein, M. L. *J. Phys. Chem. B* **2003**, *107*, 4182–4188.
(50) Ivanov, I.; Tainer, J. A.; McCammon, J. A. *Proc. Natl. Acad. Sci. U.S.A.* **2007**, *104*, 1465–1470.
(51) Amin, E. A.; Truhlar, D. G. *J. Chem. Theory Comput.* **2008**, *4*, 75–85.
(52) Zhao, Y.; Schultz, N. E.; Truhlar, D. G. *J. Chem. Theory Comput.* **2006**, *2*, 364–382.
(53) Lee, C. T.; Yang, W. T.; Parr, R. G. *Phys. Rev. B: Condens. Matter Mater. Phys.* **1988**, *37*, 785–789.
(54) Becke, A. D. *J. Chem. Phys.* **1993**, *98*, 5648–5652.
(55) Becke, A. D. *J. Chem. Phys.* **1996**, *104*, 1040–1046.
(56) Perdew, J. P. *Phys. Rev. B: Condens. Matter Mater. Phys.* **1986**, *33*, 8822–8824.
(57) Nosé, S. *J. Chem. Phys.* **1984**, *81*, 511–519.
(58) Laio, A.; Parrinello, M. *Proc. Natl. Acad. Sci. U.S.A.* **2002**, *99*, 12562–12566.
(59) Iannuzzi, M.; Laio, A.; Parrinello, M. *Phys. Rev. Lett.* **2003**, *90*, 238302.

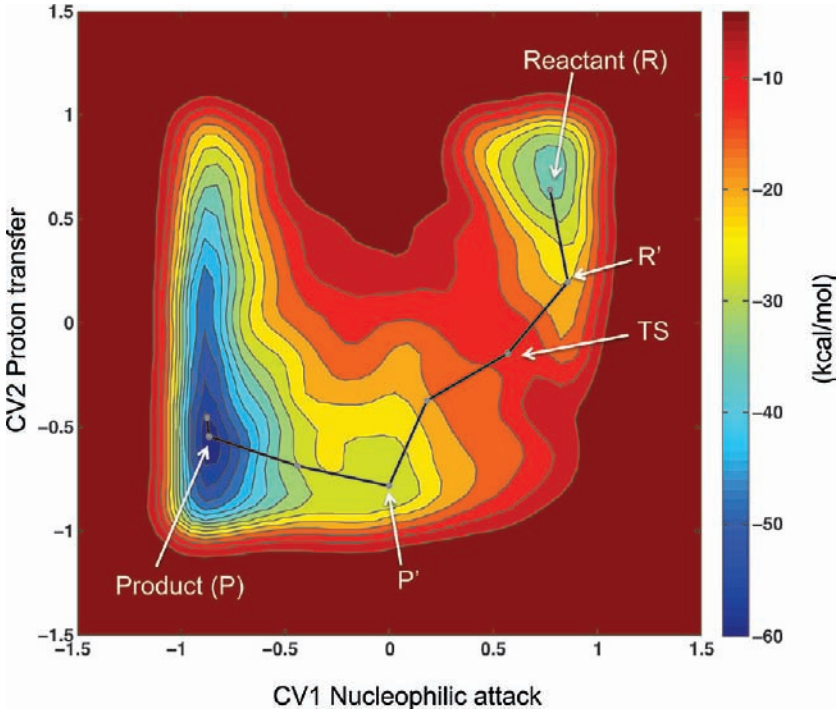


***Figure 5.*** GMII-catalyzed glycosylation free energy surface. The minimal free energy pathway is shown by gray dots connected with black lines. Contour lines are separated by 4 kcal/mol intervals.

where $d_{ij}$ is the internuclear distance of the atoms involved, $d^0$ is the threshold distance for bonding, and $p$ and $q$ are exponents that determine the steepness of $CN_{ij}$ decay with respect to $d_{ij}$. CN values range from 0 (no bond) to 1 (a bond). There are two CVs in this system: CV1 is the difference in *CN* between the scissile glycosidic bond and the bond between the nucleophile, Asp204, and the anomeric carbon atom C1′ ($CN_{C1'\text{-}O6} - CN_{C1'\text{-}OAsp204}$), while CV2 is the difference of *CN* between the $H_{Asp341}-O_{Asp341}$ and the $O6-H_{Asp341}$ bonds ($CN_{HAsp341'\text{-}OAsp341} - CN_{HAsp341'\text{-}O6}$). The latter models the proton transfer between the catalytic acid/base, Asp341, and the scissile glycosidic oxygen atom. The selected values for the *CN* parameters were $d^0 = 4.72$ au, $p = 10$, and $q = 6$ for CV1, and $d^0 = 2.55$ au, $p = 14$, and $q = 6$ for CV2.

An extended Lagrangian version of the method is here used for a proper coupling with the QM/MM simulations (SI).[40,59] The selected mass values of the fictitious particles were 15 and 5 amu for CV1 and CV2, respectively, while those of the force constant were 1.3 and 1.5 au, respectively, for CV1 and CV2. The height of the Gaussian terms was 1.25 kcal mol$^{-1}$, which ensures sufficient accuracy for reconstructing the free energy surface. The width of the Gaussian terms (0.05 Å) was selected from the oscillations of the CVs in a free Car−Parrinello QM/MM simulation. A new Gaussian-like potential was added every 300 MD steps and the simulation was stopped after one recrossing of the TS. Approximately 950 Gaussian hills were added during the metadynamics simulation which, in terms of simulation time, corresponds to 35.9 ps. The simulation was performed in an AMD Opteron cluster and required about 144 000 CPU h.

## 3. Results and Discussion

**3.1. Michaelis Complex of GMII.** The initial structure of the enzyme−substrate complex was taken from the structure of *D. melanogaster* GMII (PDB 3CZN) complexed with its natural substrate. In this structure, an alanine residue replaces the nucleophile (Asp204) and the substrate Man5 mannosyl residue adopts an undistorted $^4C_1$ conformation. To model the Michaelis complex, the mutation was computationally reverted to Asp204 (Computational Methods section). This causes an interaction between the nucleophile and the active site Zn ion to appear.

During the initial MD simulation, the conformation of the substrate mannosyl ring changed spontaneously from $^4C_1$ to a distorted conformation ($B_{2,5}$), probably to avoid the unfavorable close contact between O2′ and $O_{Asp204}$ atoms (1.52 Å in the $^4C_1$ conformer but 2.75 Å in the $B_{2,5}$ one). In principle, this could be taken as a proof that the $^4C_1$ substrate conformation was due to the mutation. However, it should be pointed out that in some cases classical force fields fail to reproduce the distortion of the substrate in GHs.[60] To take a step forward in accuracy and predictive power, we recomputed the structure of the Michaelis complex by QM/MM (see details in the Computational Methods section), that is, taking into account electronic effects and charge rearrangements in the active site. The structure of the Michaelis complex of GMII obtained from QM/MM optimization is shown in Figure 3b. The conformation of the mannosyl ring ($^OS_2/B_{2,5}$) is similar to the one predicted by the classical simulation. Therefore, both classical and QM/MM simulations show that the $^4C_1$ conformation of the M5 substrate mannosyl ring in the D204A mutant of GMII is due to the mutation, and that the real substrate conformation in the Michaelis complex is intermediate between $^OS_2$ and $B_{2,5}$.

**3.2. Simulation of the Glycosylation Reaction.** The metadynamics method was used to model the GMII-catalyzed glycosylation step during hydrolysis of the α-1,6 glycosidic bond that links the Man3 and Man5 residues in $GlcNAcMan_5GlcNAc_2$ (Figure 1). The collective variables, CV1 and CV2, used in the simulation give an idea of the degree of formation of the covalent bond between the substrate and the nucleophile residue (CV1) and the proton transfer between the acid/base residue

(60) Biarnes, X.; Nieto, J.; Planas, A.; Rovira, C. *J. Biol. Chem.* **2006**, *281*, 1432–1441.

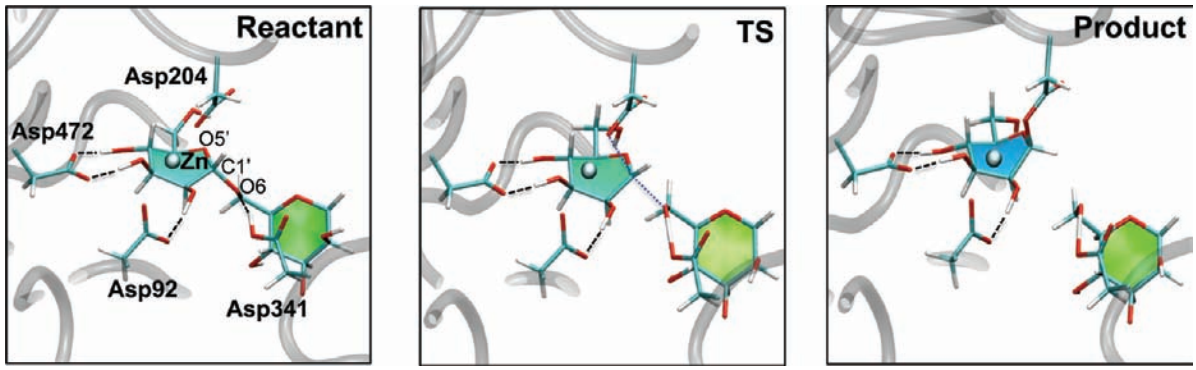


***Figure 6.*** Snapshots along the reaction pathway. The Zn ligands (His90 and His471, Figure 3) have been omitted for clarity.

***Table 1.*** Lengths (Å) of Important Bonds along the Reaction Pathway

| bond | reactant (R) | R′ | TS | P′ | product (P) |
|---|---|---|---|---|---|
| C1′−O6 | 1.53 ± 0.05[a] | 1.56 ± 0.06 | 2.00 ± 0.23 | 2.57 ± 0.10 | 3.47 ± 0.11 |
| C1′−$O_{Asp204}$ | 3.25 ± 0.06 | 3.25 ± 0.12 | 2.93 ± 0.11 | 2.56 ± 0.14 | 1.50 ± 0.04 |
| $O_{Asp341}$−$H_{Asp341}$ | 1.03 ± 0.03 | 1.12 ± 0.06 | 1.27 ± 0.02 | 1.73 ± 0.05 | 1.56 ± 0.03 |
| $H_{Asp341}$−O6 | 1.74 ± 0.05 | 1.35 ± 0.04 | 1.19 ± 0.03 | 1.02 ± 0.03 | 1.03 ± 0.02 |
| C1′−O5′ | 1.41 ± 0.03 | 1.40 ± 0.03 | 1.32 ± 0.03 | 1.29 ± 0.02 | 1.41 ± 0.04 |
| O2′−H2′ | 1.04 ± 0.02 | 1.04 ± 0.03 | 1.03 ± 0.04 | 1.06 ± 0.05 | 1.03 ± 0.03 |
| H2′−$O_{Asp92}$ | 1.55 ± 0.11 | 1.56 ± 0.10 | 1.56 ± 0.09 | 1.51 ± 0.13 | 1.60 ± 0.14 |
| Zn−$O_{Asp204}$ | 2.12 ± 0.06 | 2.10 ± 0.08 | 2.11 ± 0.09 | 2.19 ± 0.14 | 3.00 ± 0.08 |
| Zn−$O_{Asp92}$ | 2.37 ± 0.13 | 2.28 ± 0.12 | 2.23 ± 0.10 | 2.26 ± 0.12 | 2.08 ± 0.07 |
| Zn−$N_{His90}$ | 2.17 ± 0.05 | 2.15 ± 0.07 | 2.18 ± 0.07 | 2.10 ± 0.07 | 2.12 ± 0.06 |
| Zn−$N_{His471}$ | 2.13 ± 0.08 | 2.15 ± 0.07 | 2.18 ± 0.08 | 2.13 ± 0.07 | 2.11 ± 0.06 |
| Zn−O2′ | 2.27 ± 0.06 | 2.35 ± 0.13 | 2.46 ± 0.16 | 2.29 ± 0.11 | 2.24 ± 0.10 |
| Zn−O3′ | 2.32 ± 0.07 | 2.34 ± 0.16 | 2.37 ± 0.11 | 2.39 ± 0.11 | 2.26 ± 0.11 |

[a] Standard deviation.

***Table 2.*** Average Restrained Electrostatic Potential Charges[63] of Relevant Atoms along the Reaction Pathway

| atom | reactant (R) | R′ | TS | P′ | product (P) |
|---|---|---|---|---|---|
| C1′ | 0.51 ± 0.12[a] | 0.51 ± 0.15 | 0.61 ± 0.03 | 0.51 ± 0.11 | 0.56 ± 0.07 |
| O5′ | −0.65 ± 0.07 | −0.58 ± 0.10 | −0.41 ± 0.05 | −0.32 ± 0.08 | −0.57 ± 0.10 |
| O6 | −0.41 ± 0.04 | −0.48 ± 0.14 | −0.66 ± 0.06 | −0.74 ± 0.05 | −0.81 ± 0.07 |
| O2′ | −0.55 ± 0.11 | −0.59 ± 0.12 | −0.52 ± 0.06 | −0.48 ± 0.11 | −0.52 ± 0.07 |
| $O_{Asp204}$ | −0.83 ± 0.12 | −0.83 ± 0.06 | −0.74 ± 0.07 | −0.71 ± 0.05 | −0.54 ± 0.03 |
| $O_{Asp341}$ | −0.68 ± 0.08 | −0.76 ± 0.04 | −0.88 ± 0.05 | −0.92 ± 0.03 | −0.90 ± 0.03 |
| Zn | 0.83 ± 0.22 | 0.82 ± 0.20 | 0.61 ± 0.14 | 0.51 ± 0.13 | 0.69 ± 0.15 |
| $\delta^{an}$ [b] | 0.23 | 0.25 | 0.37 | 0.40 | 0.09 |

[a] Standard deviation. [b] Sum of charges of C1′, C2′, H1′, and O5′ atoms.

and the substrate glycosidic oxygen (CV2). The evolution of the CVs during the complete simulation is shown in SI Figures S3 and S4.

The free energy surface (FES) obtained from the metadynamics simulation is shown in Figure 5. Here, the relevant stationary points corresponding to reactant, TS (the maximal energy point along the reaction pathway), and product (the covalent intermediate) states can be identified. The calculated reaction free energy of activation is ∼23 kcal/mol, which agrees well with the experimentally measured free energy of activation of 20 kcal/mol (obtained from the hydrolysis rate constant) for GH38 *Aspergillus fischeri* α-mannosidase hydrolyzing the α-Man-(1→6)-Man bond.[61] The exothermicity of the reaction, computed as the free energy between the Michaelis complex and covalent intermediate, is ∼22 kcal/mol.

A detailed description of the glycosylation reaction in GMII was obtained by following the minimal free energy pathway, as given by the intrinsic reaction coordinate.[62] Snapshots of average structures for the reactant, TS, and product states are shown in Figure 6. At the reactant state, the catalytic acid/base (Asp341) is in its protonated state, forming a hydrogen bond (1.74 Å) with the glycosidic oxygen atom (O6). When the reaction starts, the nucleophile (Asp204) is in its charged state and is significantly separated (3.25 Å) from the C1′ atom (Table 1). Two additional carboxylate groups form strong hydrogen bonds with the glycol. Asp92 interacts with the C2′−OH hydroxyl group and Asp472 forms a bidentate interaction with the C3′−OH and C4′−OH groups. The zinc ion is hexacoordinated by His90, Asp92, Asp204, His471, and two substrate oxygen atoms, O2′ and O3′, as previously observed in the crystal structures.[19]

The reaction begins with the Asp341 O−H bond lengthening along the minimal free energy pathway from the reactant state (R) to R′ (Figure 5), indicating partial transfer of the Asp341 proton. At R′, the Asp341 proton is 1.35 Å from the O6 glycosidic oxygen atom (Table 1). The system then reaches the TS when the scissile bond elongates to ∼2 Å and the distance between the nucleophile, Asp204, and the C1′ atom shortens from 3.25 Å in the reactant state to 2.93 Å in the TS. The

(61) Shashidhara, K. S.; Gaikwad, S. M. *Int. J. Biol. Macromol.* **2009**, *44*, 112–115.
(62) Fukui, K. *Acc. Chem. Res.* **1981**, *14*, 363–368.

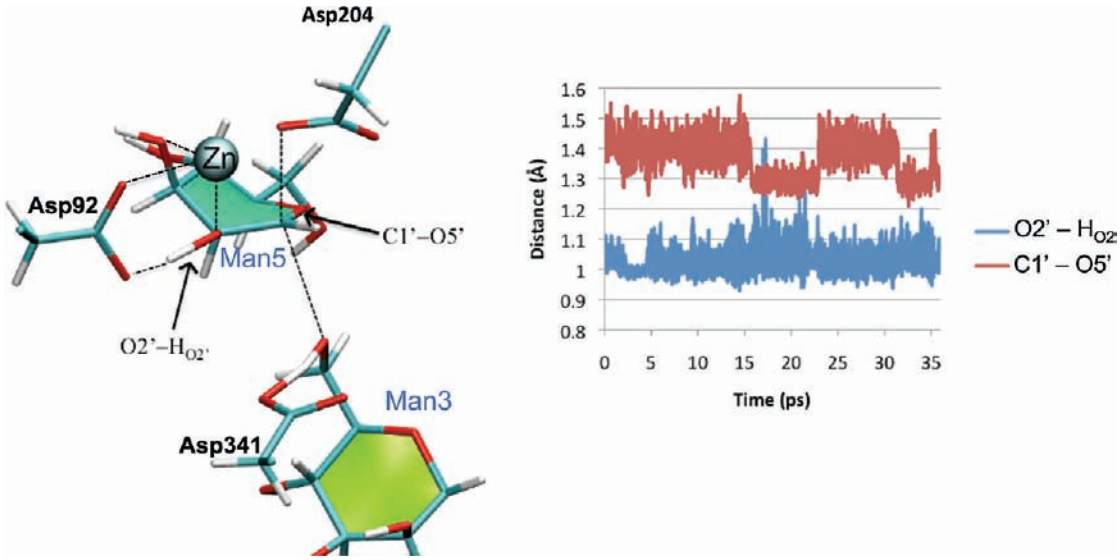


***Figure 7.*** Variation of the C1′−O5′ and O2′−H$_{O2'}$ distances throughout the metadynamics simulation. The O2′−H$_{O2'}$ distance increases upon formation of the OCI-like species, which is represented by a decrease of the C1′−O5′ distance. It is important to note that metadynamics time does not represent real time.

Asp341 proton transfers further to within 1.19 Å of O6. In addition, the intraring C1′−O5′ bond shrinks significantly from 1.41 Å in the reactant state to 1.32 Å in the TS, indicating the formation of a partial double bond and the increasing oxacarbenium ion (OCI) character of the mannosyl substrate.

The substrate is expected to reach its maximal OCI character at CV1 = 0, where both the C1′−O$_{Asp204}$ and C1′−O6 bonds are broken (i.e., their coordination numbers vanish). This corresponds to P′ in the FES (Figure 5). At this point, both the nucleophile and leaving group are ∼2.5 Å from the C1′ atom. The C1′−O5′ distance reaches a minimum (1.29 Å), and the C1′ atom becomes sp2-hybridized. Interestingly, the TS does not coincide with the point of maximal OCI character (P′) but is closer to the reactants (Figure 5). Therefore, the simulation shows that the glycosylation reaction in GMII follows a $D_NA_N$ mechanism, where the nucleophilic attack occurs before the scissile glycosidic bond is fully broken.[23]

To quantify the degree of OCI character in the mannosyl residue along the reaction, a partial charge analysis was performed (Table 2).[63] Since the charge increase of the anomeric carbon atom along the reaction pathway delocalizes over its neighboring atoms, especially at O5′, we summed up the charges of C1′, O5′, C2′, and H1′ atoms ($\delta^{an}$) (Table 2). As expected from the shape of the FES, the maximal value of $\delta^{an}$ does not occur at the TS but at P′. As the reaction progresses from R to the TS and further to P′, $\delta^{an}$ increases by 0.17 electrons, mainly due to the change at the ring oxygen atom (O5′). Interestingly, the Zn ion charge shows the opposite tendency (Figure S5, SI). Thus, the increase in anomeric charge is compensated by a decrease of positive charge of the Zn ion. This clearly indicates that the role of Zn is not just structural but is also catalytic.

Finally, in the product state, a covalent bond between Asp204 and the C1′ atom is formed (1.5 Å). At this point, the leaving group is completely dissociated (C1′···O6 = 3.47 Å), the anomeric carbon atom has recovered its sp3-hybridization, and the C1′−O5′ distance is as short as in the reactant state (1.41 Å). Following the reaction coordinate from reactant to product,

(63) Bayly, C. I.; Cieplak, P.; Cornell, W. D.; Kollman, P. A. *J. Phys. Chem.* **1993**, *97*, 10269–10280.

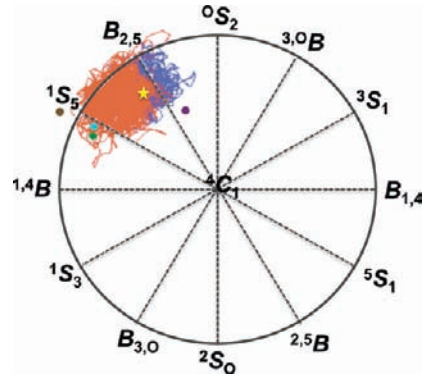


***Figure 8.*** Conformational itinerary of the glycon mannosyl ring along the metadynamics simulation, mapped onto a Cremer-Pople sphere. The conformations visited before the TS are shown in blue, while those visited after the TS are shown in red. The average TS conformation is shown with a yellow star. The experimentally observed conformation for the Michaelis complex in a mutated (D341N) GMII enzyme is shown with a purple dot (PDB 3BUP). Three conformations corresponding to enzyme-covalent intermediate structures are shown as brown (PDB 1QX1), green (PDB 1QWU), and light blue (PDB 1QWN) dots.

the nucleophilic oxygen atom (O$_{Asp204}$) loses electronic charge as the nucleophile forms a covalent bond with the C1′ atom (Table 2). In contrast, the leaving group oxygen atom (O6) becomes more negative during the reaction pathway. The formation of the covalent bond between the glycon and Asp204 lengthens the O$_{Asp204}$···Zn distance from 2.12 to 3.00 Å (Table 1), which is compensated by a decrease of the distances between Zn and the rest of its coordinating atoms.

**3.3. Role of Zinc and Partial Deprotonation of the O2′−H$_{O2'}$ Bond.** As mentioned in the Introduction, the presence of a catalytic Zn ion in the active site of GHs is unprecedented, and its precise role remains unclear. The Zn ion is coordinated with both O2′ and O3′ glycon atoms of the substrate (Figure 3b). The Lewis acid character of the Zn ion could allow withdrawal of electrons from the substrate,[29] but this would adversely affect the formation of electron-deficient OCI-like species.

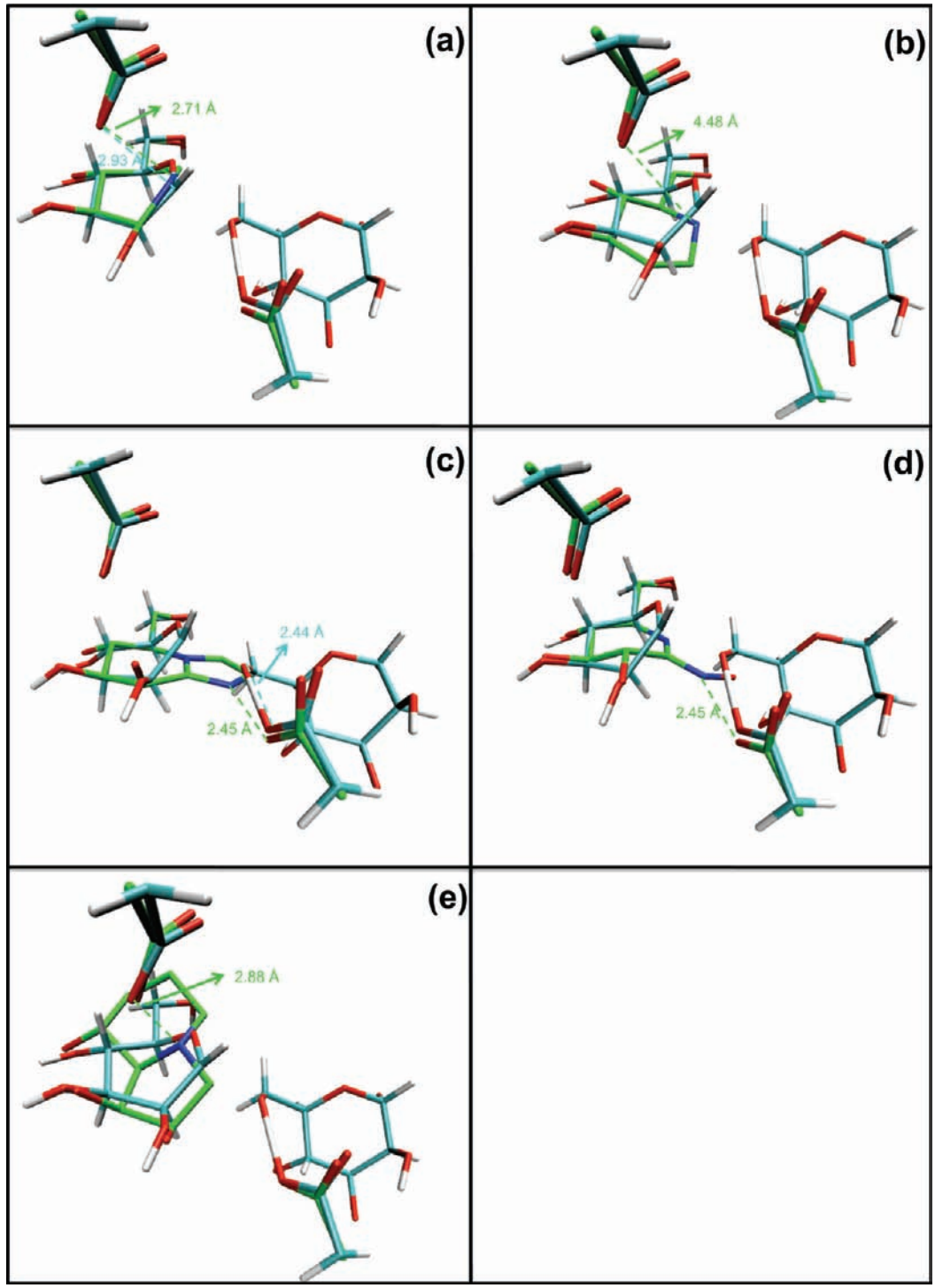


***Figure 9.*** Superposition of GMII-TS structures and several experimentally obtained GMII-inhibitor complexes. (a) noeuromycin (PDB code 2ALW), (b) deoxymannojirimycin (PDB code 1HXK), (c) mannoimidazole (PDB code 3D4Y), (d) gluco-hydroxyiminolactam (PDB code 3D51) and (e) swainsonine (PDB code 1HWW). Blue dashed lines and numbers correspond to the TS. Green dashed lines and numbers correspond to inhibitors.

The hydrogen atom from the C2′−OH hydroxyl group forms a hydrogen bond with Asp92. It is well-known that interactions between the C2′−OH group and electron-donating groups stabilize the OCI-like TS more than interactions with other glycon hydroxyl groups do.[64] Even in solution, electron-withdrawing groups at the C2′ atom cause larger decreases in reaction rate than similar substituents at other pyranosyl ring positions.[65] This due to the C2′−OH group being close to the anomeric center, which becomes electron-deficient at the TS. In the case of $\beta$-retaining GH enzymes, where the nucleophile is hydrogen-bonded to the 2′−OH, it has been proposed[28,66] that the high acidity of the O2′ atom at the TS leads to partial deprotonation of the O2′−$H_{O2'}$ bond.

(64) Namchuk, M. N.; Withers, S. G. *Biochemistry* **1995**, *34*, 16194–16202.

(65) Namchuk, M.; McCarter, J.; Becalski, A.; Andrews, T.; Withers, S. *J. Am. Chem. Soc.* **2000**, *122*, 1270–1277.

(66) Withers, S. G. *Carbohydr. Polym.* **2001**, *44*, 325–337.

A similar situation occurs for GMII, as partial deprotonation of the O2′−$H_{O2'}$ bond upon formation of the mannosyl OCI species is observed. Figure 7 shows the time evolution of the O2′−$H_{O2'}$ and C1′−O5′ distances throughout the metadynamics simulation. A decrease of the C1′−O5′ distance indicates the formation of the mannosyl OCI-like species. Interestingly, this decrease (occurring from 15 to 25 ps) is paralleled by an increase of the O2′−$H_{O2'}$ distance. At a certain point (∼17 ps of the simulation), the O2′−$H_{O2'}$ bond breaks and the $H_{O2'}$ proton transfers to Asp92. The partial deprotonation of the O2′ atom provides electrons that can be delocalized to the anomeric center, producing a stabilizing effect. Since the Zn ion is coordinated to the O2′ atom, it stabilizes the negative charge accumulated on the latter upon lengthening of the O2′−H bond, thus indirectly relieving the electronic deficiency of the OCI-like species. In fact (section 3.2), the charge of the Zn ion varies in concert with the anomeric charge (Table 2, Figure S5, SI), indicating that the positive charge of the Zn ion is tuned to appropriately stabilize the O2′ atom without destabilizing the OCI species. Therefore, our results indicate that the interaction of the Zn ion and O2′ atom is relevant for catalysis in GMII.

**3.4. Conformational Itinerary of the Glycon Mannosyl Ring along the Reaction Path.** The conformational itinerary of the glycon mannosyl ring along the reaction path was analyzed by monitoring the ring conformation during the metadynamics simulation. Figure 8 shows a two-dimensional projection of the Cremer-Pople[67] sphere (also named the Stoddart diagram) viewed from the North Pole that shows many of the possible puckering conformations of a pyranosyl ring. The mannosyl ring conformations visited before the TS (shown in blue) lie around the $B_{2,5}$ conformation, slightly protruding into the $^{O}S_2$ region. The conformations visited after the TS are shown in red, populating the zone between the $B_{2,5}$ and $^{1}S_5$ conformations. Experimental points for the Michaelis complex and enzyme-mannosyl covalent intermediate are also plotted onto the Stoddart diagram for comparison. The average conformation found for the TS structures is close to a $B_{2,5}$ (the yellow star in Figure 8). Therefore, our simulations show that GMII follows an $^{O}S_2/B_{2,5} \rightarrow B_{2,5}$ [TS] $\rightarrow {}^{1}S_5$ itinerary for the glycosylation step.

**3.5. Comparison between GMII-TS and GMII-Inhibitor Structures.** As mentioned in the Introduction, inhibition of GMII has shown promise against certain types of cancer. It is well-known that TS analogs are powerful enzyme inhibitors; therefore, we carried out a comparison between the GMII-TS structure obtained in this work and several GMII inhibitors recently solved by Rose and co-workers.[15,18]

Figure 9 shows the result of superimposing the active sites of five different GMII crystal structures complexed with inhibitors to the GMII-TS structure. Figure 9a and b shows the GMII-TS structure compared to noeuromycin and deoxymannojirimycin, respectively. Noeuromycin is a much better inhibitor than the chemically similar deoxymannojirimycin (the former has a positively charged NH group in place of the anomeric carbon atom, while the latter places the NH group at the ring oxygen).[29] It is clear in comparing Figure 9a and b that noeuromycin ($K_i$ = 20 mM) resembles the TS much more than does deoxymannojirimycin ($K_i$ = 400 mM). The ring in noeuromycin is distorted toward a $^{1}S_5$-like conformation and the NH···$O_{Asp204}$ (2.71 Å) distance mimics the one observed at the TS (2.93 Å for C1′···$O_{Asp204}$). On the other hand, the ring in deoxymannojirimycin is not distorted when bound to the enzyme, and the positively charged inhibitor's NH group is positioned far away from the nucleophile (4.48 Å), unable to mimic the C1′···$O_{Asp204}$ distance observed at the TS.

Figure 9c and d shows a comparison between the GMII-TS and the inhibitors mannoimidazole ($K_i$ = 2 mM) and gluco-hydroxyiminolactam ($K_i$ = 70 mM).[18] The ring conformation departs appreciably from the computed TS in both cases. However, these inhibitors mimic the distance between the leaving group and the catalytic acid observed at the TS (2.44 Å for the O6···$O_{Asp341}$ bond). The analogous distance of the inhibitors (N···$O_{Asp341}$) is very close (2.45 Å) in both cases.

The most powerful GMII inhibitor known is swainsonine ($K_i$ = 0.02 mM). Its structure when complexed with GMII is shown in Figure 9e, superimposed to the TS. Swainsonine positions a five-membered ring on top of the six-membered ring of the natural substrate, and therefore it does not look like a TS analog. Nevertheless, the N···$O_{Asp204}$ distance observed in the GMII-swainsonine complex is 2.88 Å, very close to the analogous C1′···$O_{Asp204}$ distance observed at the TS (2.93 Å). The N···$O_{Asp204}$ distance observed in swainsonine is even closer to the TS than in noeuromycin, which may provide an explanation of swainsonine's higher potency. These results suggest that targeting the C1′···$O_{Asp204}$ or O6···$O_{Asp341}$ distances observed in the TS is important to design powerful inhibitors.

**3.6. Summary.** In this work, we have addressed the glycosylation reaction step during GMII-catalyzed hydrolysis of a mannosyl α-1,6 glycosidic bond by means of first-principles metadynamics simulations, providing an atomistic description of the reaction step. The computed free energy barrier of the reaction and the conformation of the Man5 mannosyl residue in the product ($^{1}S_5$) agree well with experiments. We find that the substrate adopts a $^{O}S_2/B_{2,5}$ conformation in the Michaelis complex, whereas the $^{4}C_1$ conformation observed in the 3CZN structure is due to mutation of the nucleophile. Glycosidic bond dissociation occurs before formation of the covalent bond between the substrate and the nucleophile residue (i.e., a $D_NA_N$-type reaction), and the TS has a clear OCI character and displays a $B_{2,5}$ conformation. The glycosylation reaction follows an itinerary similar to $^{O}S_2/B_{2,5} \rightarrow B_{2,5}$ [TS] $\rightarrow {}^{1}S_5$, agreeing with the proposal by Rose et al. after they compared α- and β-mannanases.[16] Because TS analogs are powerful inhibitors, the structural and electronic features of the TS presented in this work can be used to guide inhibitor design. More specifically, a comparison of the TS structure obtained from the calculations and the structure of recently formulated GMII inhibitors reveals that the best inhibitors are the ones that best mimic the C1′···$O_{Asp204}$ and O6···$O_{Asp341}$ interactions. These results suggest that targeting both of these interactions in the same molecule could lead to more powerful inhibitors. The simulations also suggest a mechanism to explain the previously proposed catalytic role of Zn; in particular, it helps to lengthen the O2′−$H_{O2}$ bond when the substrate acquires OCI character, relieving the electron deficiency of the OCI-like species. Confirmation of this proposal awaits appropriate experimental data.

**Acknowledgment.** We thank the Iowa State University High Performance Computation System for making its facilities available to us. We also thank the National Research Initiative of the U.S. Department of Agriculture Cooperative State Research, Education and Extension Service (grant number 2007-35504-18252), the Generalitat de Catalunya (grant 2009SGR-1309), and the Ministerio

(67) Cremer, D.; Pople, J. A. *J. Am. Chem. Soc.* **1975**, *97*, 1354–1358.

de Ciencia e Innovación (MICINN) (grant FIS2008-03845) for its financial assistance. A.A. acknowledges an FPU research fellowship from MCINN.

**Supporting Information Available:** More extensive explanation of the metadynamics simulation, a scheme of the N-linked glycosylation pathway (Figure S1) and additional computational details and system evolution during the metadynamics simulation (Figures S3 and S4). Figure S5 shows the synchronous variation of the Zn and anomeric charges. Table S1 shows B-factors of active-site atoms. Figure S2 shows the overlap of crystal-structure and QM/MM minimized structure (after equilibration). Figure 6 shows the charge variation during the reaction pathway calculated with different DFT functionals. This material is available free of charge via the Internet at http://pubs.acs.org.

JA909249U